J. COMBIN. MATH. COMBIN. COMPUT. 127b (2025) 4003--4027

Journal of Combinatorial Mathematics and Combinatorial Computing
www.combinatorialpress.com/jcmcc

Combinatorial Press

Geometric Algebra-Based Modeling Techniques for 3D Animation and Their Application to Visual Communication

Yi Cui[1, ✉]

[1] *Zhengzhou Railway Vocational & Technical College, Zhengzhou, Henan, 450000, China*

ABSTRACT

The article constructs binocular vision 3D image structure by feature extraction and data acquisition of animated images, setting the base modeling points multi-level, establishing texture mapping modeling relationship, then designing key frame interpolation algorithms such as segmented cubic spline interpolation and quaternionic spherical linear interpolation, and applying geometric algebra to 3D animation modeling, and using a conformal geometric algebra approach to describe the 3D model as well as the dynamic model. Calculation results. The 3D animation modeling using the method of this paper reduces the error of 36.8mm compared with the same type of method, so the effect of using the method of this paper is better than 1other algorithms in 3D human body modeling. In the subjective evaluation of the visual effect of 3D animation video, 19 people think that the video has a strong sense of spatial three-dimensionality, and on the whole, the majority of people think that the animation video developed using the method of this paper is clear, realistic, has a sense of spatial three-dimensionality, smooth movement of the object, and the use of the lens is comfortable, which has a better visual communication effect.

Keywords: Geometric algebra, 3D modeling, 3D animation, visual communication, key frame interpolation algorithm

1. Introduction

Since the development of computers, 3D modeling technology has become an important part of computer graphics. 3D modeling technology is based on the principle of CAD technology, through the computer software to simulate the shape and structure of buildings, parts or products in three-dimensional space, to produce 3D models [1-4]. 3D modeling technology is mainly divided into two ways: polygonal method and NURBS method. From the initial simple wireframe drawing, to the current high-precision real-time rendering, 3D modeling technology has evolved from graphics and animation production to game development, virtual reality, medicine, architecture, visual communication and

✉ Corresponding author.
E-mail address: cuiyi7777777@163.com (Y. Cui).
Received 15 January 2024; Revised 25 March 2024; Accepted 15 December 2024; Published Online 16 April 2025.
DOI: 10.61091/jcmcc127b-222
© 2025 The Author(s). Published by Combinatorial Press. This is an open access article under the CC BY license (https://creativecommons.org/licenses/by/4.0/).

many other fields [5-8].

Visual communication refers to the art and technology of conveying information, expressing ideas, and arousing audience interest through visual elements. Visual communication has a wide range of applications in various fields, such as graphic design, advertising, publicity, exhibition and so on. The purpose of visual communication is to help people understand and receive information [9-11]. Through the use of design, typography, color scheme and other techniques, the information is transmitted to the audience in the most intuitive, accurate and attractive way. The effect of visual communication often depends on the skill and creativity of designers, who need to create visually appealing works through artistic and design means [12-14]. The elements of visual communication include image, text, color, layout, proportion and so on. These elements play different roles in visual communication. Images can visually communicate information and increase the attractiveness of the work. Text can be used to express ideas, explain images, and make information clearer. Color, on the other hand, can create different moods and atmospheres. Layout and proportion can affect the overall effect and visual balance of the work [15-18].

The article firstly proposes a 3D modeling method for animated images based on binocular vision. Through animated image feature extraction and data acquisition, the base modeling points are set to be multi-layered. Secondly, the texture mapping modeling relationship is established to construct the binocular vision 3D image structure. Then the relevant theories needed for the key frame animation system are studied, and the principle of model transformation in three-dimensional space is investigated, and the computational process of using n+1-dimensional vectors instead of the original n-dimensional vectors for coordinate operations is specifically analyzed. Subsequently, the key algorithms in the animation system are studied and designed. In the key frame interpolation algorithm section, the segmented cubic spline interpolation algorithm for common animation productions and the quaternion spherical linear interpolation algorithm for specific rotating animations are designed, and the optimization method of fold resampling for segmented cubic spline interpolation and the optimization method of intermediate frame data are innovatively designed. The algebraic method of conformal geometry is further applied to 3D animation modeling. The modeling algorithms designed in this paper are discussed and compared in detail, and the visual effects of 3D animation are analyzed from both subjective and objective aspects.

2. Method

2.1. 3D animation modeling based on binocular vision

2.1.1. Animated Image Feature Extraction and Data Acquisition. Taking the animated image face as an example, the face animation data as well as the information can be divided into head pose and muscle formation local motion. Before measurement, the monitoring node is utilized to collect the data related to the initial head pose for subsequent use.

Set up several groups of simple animated character head movements, calibrate 4 comparison points, separate the head change specifics and pure expression data, extract the animated character image features, and summarize the data change rule. Set the point frame coordinate as $v=(x,y,z,1)$, reverse point frame coordinate as $vk=(xk,yk,zk,1)$, set the specific change capture matrix, according to the character head posture change characteristics, can get the animation image description constant value, expression is:

$$H=(1-m)h+\sum_{i=1} hi\times\varpi^2 \tag{1}$$

Where: H is the animated image description constant value. m is the directional description reference value. h is the conversion description ratio. i is the number of description times. ϖ is the controllable frame value [19]. According to the change law of the key point data, estimate the fixed-point motion vectors of other positions, and adopt the spherical parameterization processing to expand the acquisition range of the animation image processing data interpolation. Setting the change local area, adjusting the coordinates of the center of gravity of 3D modeling, completing the animation image extraction and data acquisition.

2.1.2. Multi-level setting of base modeling points.The binocular vision technique was utilized to set the modeling points, and the structure of the binocular vision rotation simulation is shown in Figure 1.

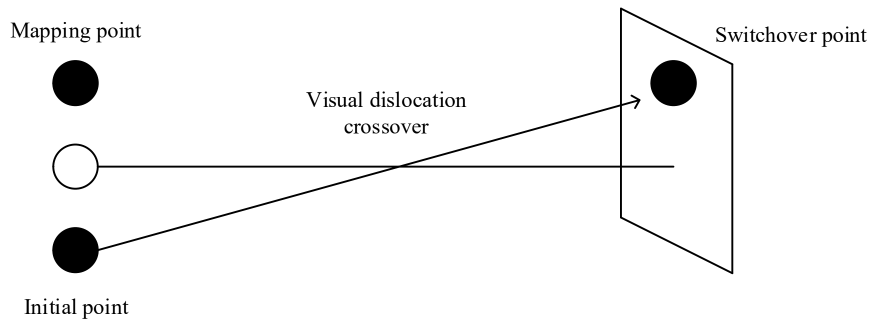

Fig. 1. Binocular vision rotation simulation structure

Construct a dynamically localized moving space with core point settings associated with external point locations to form an initial texture relationship. Calculate the predicted distance of the modeled point units with the expression:

$$K = \varphi^2 \times \frac{Q(1-C)}{SQ+t} - S \tag{2}$$

Where: K is the unit prediction distance. φ is the controllable prediction position. S is the visual deviation. Q is the visual point spacing. t is the correlation direction. C is the simulated fixed value.

2.1.3. Establishing texture mapping modeling relationships. Texture mapping is a multi-dimensional dynamic point transformation link and a key modeling execution relationship. Set the corresponding key mapping nodes in the base texture image, use 3D scanning equipment to mark the key positions of the animation image, divide the overlapping space and extents positions, set the allocation rate and the initial sequence of the animation graphics, set the geometric 3D correction structure through the lenses of different angles, and wait for the image to reach the preset clear standard to eliminate the discontinuous points and gaps. Take the sequence as a guide, set the corresponding texture mapping structure, use the capture matrix constructed above to carry out intelligent texture processing for each region, correct the focus position or line diversity position, and realize the affine transformation.

2.1.4. Constructing a three-dimensional image processing structure for binocular vision. After the texture mapping is established, the binocular vision technique is utilized to establish the 3D image processing structure. Calculate the base gradient of the image, set the edge points of the second stage, form the contour line between the points, construct the Snake model, and establish the continuous smooth closed contour structure.

Set the base animation image conversion target, find the target object boundary position, adjust the optimal standard, use the closure curve and the base model to summarize the law, when the texture mapping point positions appear in a continuous manner, discretize the Snake model to process, calibrate the binocular vision processing deviation points, drag the contour curves to the respective edge region, continue to binarize the image, set the binocular vision three-dimensional image processing structure [20]. Comprehensive image processing needs and changes in the standard, adjust the minimization energy function, set the image three-dimensional modeling approximation edge value, further enhance the stability and reliability of the structure, and strengthen the practical application performance of three-dimensional modeling.

2.2. Key Algorithm Implementation for 3D Animation System

2.2.1. Three-dimensional coordinate transformation theory:

1) Three-dimensional translation. Three-dimensional space can be assumed to be a three-dimensional coordinate system, and each point in three-dimensional space has its own unique three-dimensional coordinates. The three-dimensional coordinates of a point are represented by vector (x, y, z). If this point is translated in the three-dimensional coordinate system, the three coordinate components of the translation are dx, dy, dz, and the coordinates after translation are (x', y', z'). The transformation process from (x, y, z) to (x', y', z') can be described as equation (3):

$$\begin{aligned} x' &= x + dx \\ y' &= y + dy \\ z' &= z + dz \end{aligned} \tag{3}$$

Then there exists a translation matrix M such that $A_n = MA_m$. It is not possible to find a correct M for which the above equation holds if only for three-dimensional matrices, so the theory of three-dimensional transformations makes use of chi-square coordinates. The chi-square coordinates will specify a $n+1$-dimensional vector to represent the original n-dimensional vector, so that the coordinates in the 3-dimensional coordinate system are represented by $(x, y, z, 1)$. The matrix form of the three-dimensional translation equation can be obtained:

$$\begin{pmatrix} x' \\ y' \\ z' \\ 1 \end{pmatrix} = \begin{pmatrix} 1 & 0 & 0 & dx \\ 0 & 1 & 0 & dy \\ 0 & 0 & 1 & dz \\ 0 & 0 & 0 & 1 \end{pmatrix} \cdot \begin{pmatrix} x \\ y \\ z \\ 1 \end{pmatrix} \tag{4}$$

2) Three-dimensional rotation. Compared with translation in three-dimensional space, the principle of three-dimensional rotation is more difficult and the situation is more complicated. There are three standard axes in three-dimensional space, X, Y, Z, as well as arbitrary axes in any direction, and if you want to carry out three-dimensional rotation, you have to determine the rotation axis and rotation angle of the rotation operation. The realization of rotation in three-dimensional space is obtained by a series of combined operations of sine and cosine functions, to rotate around the x-axis as an example, set the rotation angle as θ, the rotation of its coordinates transformation formula:

$$\begin{aligned} x' &= x \\ y' &= y\cos\theta - z\sin\theta \\ z' &= y\sin\theta + \cos\theta \end{aligned} \tag{5}$$

Writing the coordinates of the point in four-dimensional matrix form gives.

Rotate around the x-axis:

$$\begin{pmatrix} x' \\ y' \\ z' \\ 1 \end{pmatrix} = \begin{pmatrix} 1 & 0 & 0 & 0 \\ 0 & \cos\theta & -sin\theta & 0 \\ 0 & \sin\theta & \cos\theta & 0 \\ 0 & 0 & 0 & 1 \end{pmatrix} \cdot \begin{pmatrix} x \\ y \\ z \\ 1 \end{pmatrix} \tag{6}$$

Rotate around the Y-axis:

$$\begin{pmatrix} x' \\ y' \\ z' \\ 1 \end{pmatrix} = \begin{pmatrix} \cos\theta & 0 & \sin\theta & 0 \\ 0 & 1 & 0 & 0 \\ -\sin\theta & 0 & \cos\theta & 0 \\ 0 & 0 & 0 & 1 \end{pmatrix} \cdot \begin{pmatrix} x \\ y \\ z \\ 1 \end{pmatrix} \tag{7}$$

Rotate around the Z-axis:

$$\begin{pmatrix} x' \\ y' \\ z' \\ 1 \end{pmatrix} = \begin{pmatrix} \cos\theta & -\sin\theta & 0 & 0 \\ \sin\theta & \cos\theta & 0 & 0 \\ 0 & 0 & 1 & 0 \\ 0 & 0 & 0 & 1 \end{pmatrix} \cdot \begin{pmatrix} x \\ y \\ z \\ 1 \end{pmatrix} \tag{8}$$

After derivation, let the rotation axis be the vector $\vec{a}$, θ is the angle of rotation and the rotation matrix is shown in equation (9):

$$\begin{pmatrix} a_x^2(1-\cos\theta)+\cos\theta & a_x a_y(1-\cos\theta)-a_z\sin\theta & a_x a_z(1-\cos\theta)+a_y\sin\theta & 0 \\ a_x a_y(1-\cos\theta)+a_z\sin\theta & a_y^2(1-\cos\theta)+\cos\theta & a_y a_z(1-\cos\theta)-a_x\sin\theta & 0 \\ a_x a_z(1-\cos\theta)-a_y\sin\theta & a_y a_z(1-\cos\theta)+a_x\sin\theta & a_z^2(1-\cos\theta)+\cos\theta & 0 \\ 0 & 0 & 0 & 1 \end{pmatrix} \tag{9}$$

3) Three-dimensional scaling. In three-dimensional space, scaling is performed for a certain point $P(x,y,z)$, and let $S(x),S(y),S(z)$ be the scaling factor of each coordinate component of the point, then its scaling formula is shown in equation (10):

$$\begin{aligned} x' &= S(x)\cdot x \\ y' &= S(y)\cdot y \\ z' &= S(z)\cdot z \end{aligned} \tag{10}$$

Write this scaling formula in the chi-square form of the matrix.

$$\begin{pmatrix} x' \\ y' \\ z' \\ 1 \end{pmatrix} = \begin{pmatrix} S(x) & 0 & 0 & 0 \\ 0 & S(y) & 0 & 0 \\ 0 & 0 & S(z) & 0 \\ 0 & 0 & 0 & 1 \end{pmatrix} \cdot \begin{pmatrix} x \\ y \\ z \\ 1 \end{pmatrix} \tag{11}$$

2.2.2. Research and design of key frame interpolation algorithm:

1) Overall flow of keyframe interpolation. This subsection is mainly to analyze the overall flow of the keyframe interpolation algorithm, even though different interpolation methods are used, the flow of keyframe interpolation is the same, only in the selection of specific mathematical algorithms there are some differences [21]. The overall flow of keyframe interpolation is shown in Figure 2.

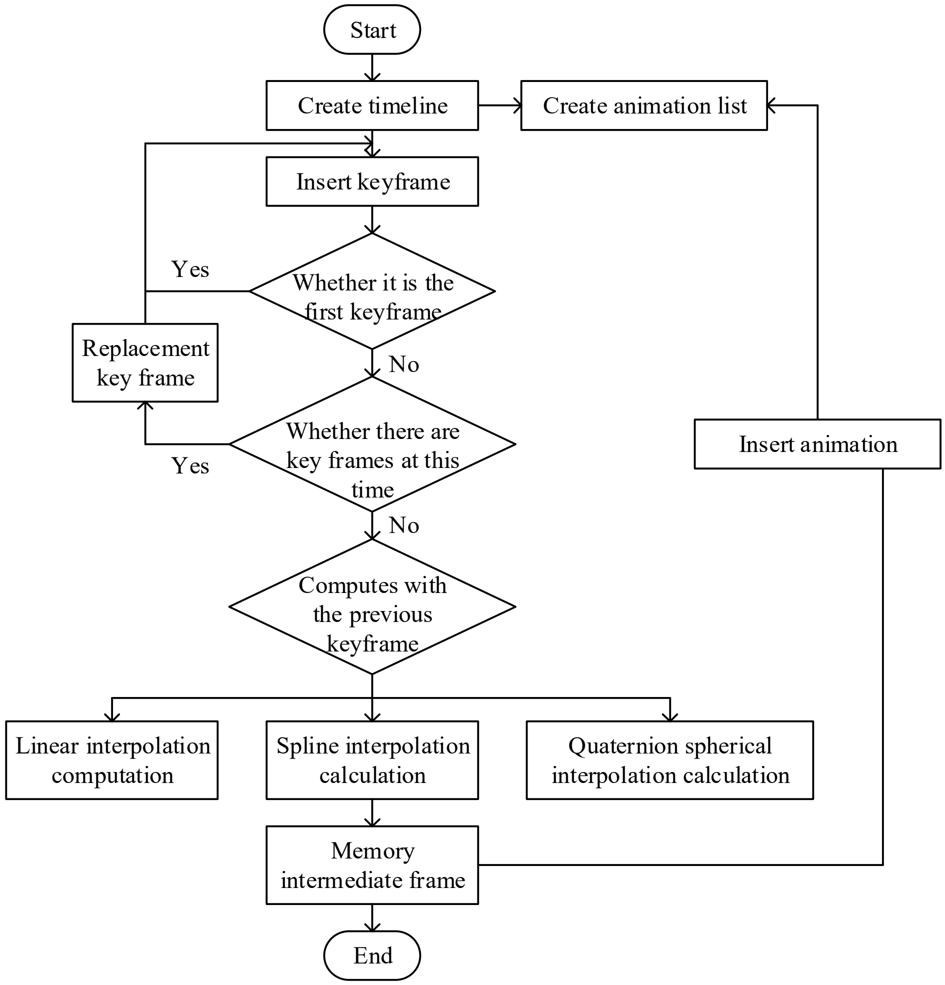

Fig. 2. Overall flow of the key frame interpolation algorithm

2) Segmented cubic spline interpolation algorithm design. In general animation software, spline interpolation is often used, so that the animation route has second-order continuity. In this system, the innovative use of segmented cubic spline interpolation, the principle is more suitable for key frame interpolation system. Segmentation is to divide the whole interval $[a,b]$ into n intervals $[(x_0,x_1),(x_1,x_2),...,(x_{n-1},x_n)]$, in which there are $n+1$ points.
1) Each interval $[x_i,x_{i+1}], S(x)=S_i(x)$ is a cubic equation where $i=0,1,\ldots n-1$.
2) Each point on the segmented interval satisfies the interpolation basis condition, viz:

$$S(x_i)=y_i \tag{12}$$

3) $S(x)$ and its first and second order derivatives are continuous.

The cubic equation can be constructed in the following form:

$$y=a_i+b_ix+c_ix^2+d_ix^3 \tag{13}$$

Call this equation the cubic spline function $S_i(x)$. where there are four unknowns for $S_i(x)$ on each small interval: (a_i,b_i,c_i,d_i). These four unknowns can be found by a finite number of conditions, and the parameters of the cubic spline interpolation equation are computed as shown in Fig. 3.

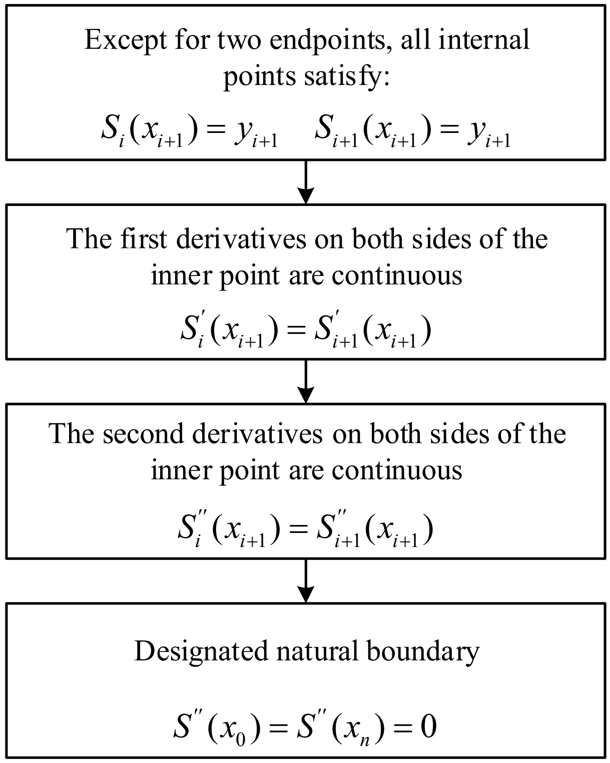

Fig. 3. Parameter calculation of cubic spline interpolation equation

While corresponding the segmented cubic spline interpolation to the keyframe animation system, in the whole animation timeline, it can be assumed that there is $n+1$ knowable keyframe data node: $(x_0, y_0),(x_1, y_1),(x_2, y_2),...,(x_n, y_n)$. Firstly, the step size is calculated as in Eq. (14) by substituting the keyframe data node and the specified beginning and end endpoint conditions into the equation.

$$h_i = x_{i+1} - x_i \tag{14}$$

By means of the matrix equations, the quadratic differential values m_i, $m_i = S_i^{''}(x_i)$. The coefficient matrix can be LU-decomposed by the Gaussian elimination method, eq:

$$B = Ax = (LU)x = L(Ux) = Ly \tag{15}$$

The coefficients of the spline curve can be obtained as:

$$\begin{aligned} a_i &= y_i \\ b_i &= \frac{y_{i+1} - y_i}{h_i} - \frac{h_i}{2} m_i - \frac{h_i}{6}(m_{i+1} - m_i) \\ c_i &= \frac{m_i}{2} \\ d_i &= \frac{m_{i+1} - m_i}{6h_i} \end{aligned} \tag{16}$$

In each subinterval $x_i \le x \le x_{i+1}$, create the equations:

$$g_i(x) = a_i + b_i(x - x_i) + c_i(x - x_i)^2 + d_i(x - x_i)^3 \tag{17}$$

3) Sample curve resampling optimization. In the segmented cubic spline interpolation process, denser interpolation points are calculated for the sake of the smoothness of the curve, which may lead to a situation of excessive data memory. Therefore, both in order to ensure the smoothness of the curve and reduce the amount of data, this paper innovatively adopts the fitting method of fold resampling

for the segmented cubic spline curve generated in the previous section, which saves the data space and ensures the accuracy of the spline curve with the minimum amount of data.

The spline curve is, in practical terms, divided into two parts in total: one is the gentle part of the curve and the other is the turning part of the curve. In the gentle part, the spline curve tends to be straight, so many interpolation points in this part are unnecessary, and the original spline curve can be fitted by a small number of interpolation points. In the turning section it is fitted with a slightly denser number of points. In this regard, due to the mutual constraints of accuracy and step size, the following judgment is used as the basis for resampling.

4) Design of Quaternion Spherical Linear Interpolation Algorithm. This system will use the quaternion spherical linear interpolation algorithm in all rotational parts. Let the moment corresponding to $\vec{p}$ be t_l, the moment corresponding to $\vec{q}$ be t_2, and the quaternion corresponding to t' be $\vec{r}$. $\vec{r}$ is the variable we require, and the scale factor t satisfies equation (18):

$$t = \frac{t' - t_1}{t_2 - t_1} \tag{18}$$

The angle between the unit quaternions $\vec{p}$ and $\vec{q}$ is θ, the angle between $\vec{p}$ and $\vec{r}$ is $t\theta$, and the angle between $\vec{q}$ and $\vec{r}$ is $(1-t)\theta$. The general interpolation formula gives the following expression for $\vec{r}$:

$$\overline{r}(t) = a(t)\overline{p} + b(t)\overline{q} \tag{19}$$

At the same time:

$$\begin{aligned} &\cos\theta = \vec{p}\cdot\vec{q} \\ &\cos(t\theta) = \vec{p}\cdot\vec{r} \\ &\cos[\,(1-t)\theta] = \vec{q}\cdot\vec{r} \end{aligned} \tag{20}$$

Joining the above equations, one can solve equation (21):

$$\begin{aligned} a(t) &= \frac{\sin[(1-t)\theta]}{\sin\theta} \\ b(t) &= \frac{\sin(t\theta)}{\sin\theta} \end{aligned} \tag{21}$$

Thus the spherical linear interpolation equation (22) is obtained:

$$Slerp\left(\vec{p},\vec{q},t\right) = \frac{\sin\left[(1-t)\theta\right]\cdot\vec{p} + \sin\left(t\theta\right)\cdot\vec{q}}{\sin\theta} \tag{22}$$

By analyzing the above various situations, when this keyframe animation system performs the rotation operation, the following algorithm flow is designed, and the flow of quaternion spherical linear interpolation algorithm is shown in Fig. 4:

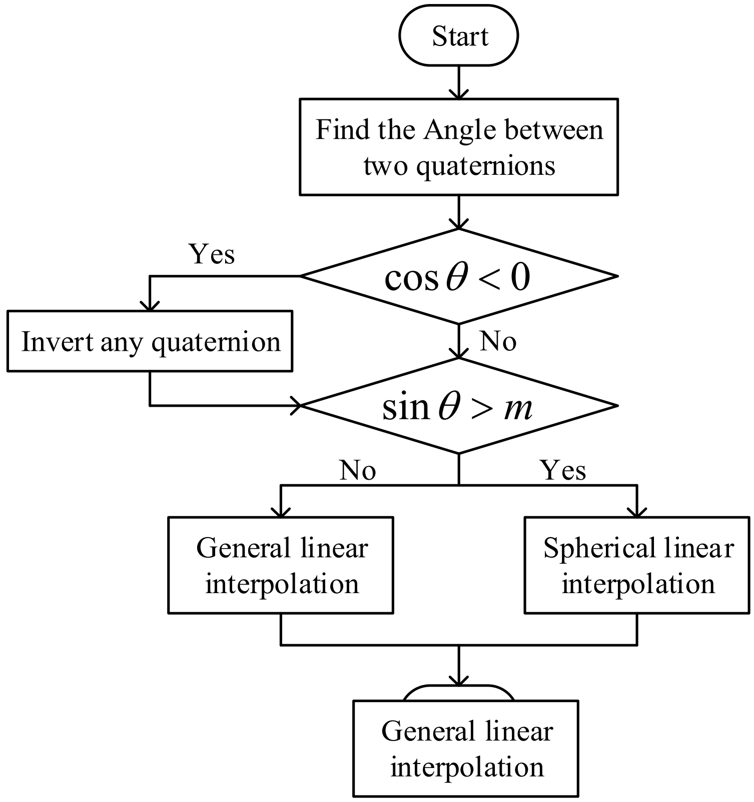

Fig. 4. Quaternion spherical linear interpolation algorithm flow

5) Optimization of intermediate frame data. Therefore, this paper innovatively designs a more ideal intermediate frame storage structure, which only needs to keep the change data of each intermediate frame relative to the key frames, and does not need to store the specific model data of the model object at the corresponding moment of the intermediate frame. The change data of each intermediate frame relative to the key frame is generated in the calculation of the interpolation algorithm of the two key frames, and the corresponding translation matrix, rotation matrix, scaling matrix, etc. can be constructed frame by frame according to the mathematical algorithm, and as long as the computed transformation matrix is applied to the original data of the model object, the intermediate frames of the model object in the corresponding moments can be obtained, and then displayed in real time. The principle of intermediate frame generation is shown in Figure 5.

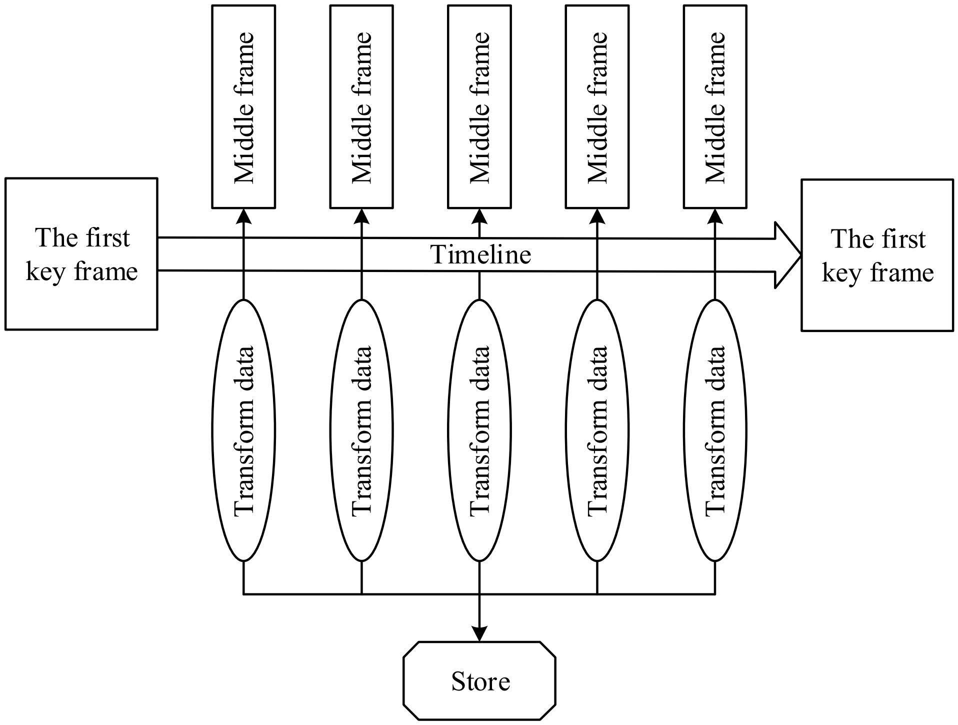

Fig. 5. Schematic diagram of generating intermediate frames

2.3. Conformal Geometric Algebra Applied to 3D Animation

2.3.1 Mathematical theory of conformal geometric algebra:

1) Introduction to Conformal Geometric Algebra. Conformal Geometric Algebra (CGA), originally known as generalized chi-square coordinates, is a new system of geometric representation and computation. As a combination of advanced invariant and covariant systems for geometry, it provides a unified and concise chi-square algebraic framework for classical geometry, as well as efficient expansion, elimination and simplification algorithms which can be used to perform extremely complex symbolic geometric computations, and it is the most practical invariant system for elementary geometry, which shows great advantages in geometric data processing and geometric computations.

2) CGA representation of rigid body motion. Rigid body motion is a transformation generated by rotations and translations in 3D space. The spinor representation of 3D rotations is introduced first.

It is well known that a rotational transformation in three-dimensional space has an invariant straight line called the axis of rotation and a set of invariant planes called the plane of rotation [22]. Every point on the rotation axis is an invariant point, and every plane perpendicular to the rotation axis is a rotation plane. The problem is that, given a set of initial poses, the corresponding terminating poses are simply obtained from the rotational transformations, and the intermediate processes are not known. Each rotation is realized in two ways: a θ-angle rotation in one direction of rotation and a $2\pi-\theta$-angle rotation in the opposite direction. In real motion, these two processes often need to be distinguished, which requires the introduction of two different representations corresponding to the same rotation, i.e., rotation representations. For three-dimensional rotations, the spin representation is exactly the quaternion representation.

Let x be a vector in a three-dimensional vector space and f be a rotational transformation, then the image of x under f is fx (a linear transformation). Let vector a be parallel to the rotational plane of f, then the spinor representation of f is $\pm R$, where:

$$R=\frac{(a+fa)a}{|a||a+fa|} \tag{23}$$

The relationship between f and R is:

$$fx = RxR^{+} \tag{24}$$

The multiplication here is the geometric product (Clifford's multiplication), $R = \frac{a(a+fa)}{|a||a+fa|}$. Let the 2-vector representation of a rotating surface with orientation past the origin be I_2 and f the angle of rotation about that orientation be θ, then $\pm R = \exp[I_2 \frac{\theta}{2}] exp[-I_2 \frac{2\pi - \theta}{2}]$ by the half-angle representation distinguishes exactly 2 different rotational processes. The Lie algebraically generated elements of a rotational quantity are called torsion quantities, as in $I_2 \frac{\theta}{2}$ in the above equation.

Eq. gives the transformation from a spinor to a rotation matrix, and the matrix form can be obtained from RxR^{+} by simply replacing x by a set of unit orthogonal bases e_1, e_2 and e_3 of R^3. On the other hand, let $f = (f_{ij}) i, j = 1,2,3$ be a rotation matrix, i.e., an orthogonal matrix with determinant equal to 1. The corresponding spinor quantity is, according to Eq:

$$\begin{aligned} \pm R &= \pm\{1 + (fe_1)e_1 + (fe_2)e_2 + (fe_3)e_3\} / \{|1 + (fe_1)e_1 + (fe_2)e_2 + (fe_3)e_3|\} \\ &= \pm\{1 + tr(f) + (f_{21} - f_{12})e_1e_2 + (f_{32} - f_{23})e_2e_3 + (f_{31} - f_{13})e_1e_3\} / \{2\sqrt{1 + tr(f)}\} \end{aligned} \tag{25}$$

Another advantage of the rotation representation is that it simplifies the parameter space of parametric rotation transformations. A rotation matrix has 9 components and satisfies 6 quadratic constraints and 1 cubic constraint. In contrast, a spinor has 4 components and satisfies 1 quadratic constraint: $RR^{+} = 1$. This has a clear advantage in parametric optimization. As a cost, the rotational transformation is linear with respect to the rotation matrix and quadratic with respect to the spinor.

Look again at the translational motion. The spinor of a translation along the displacement vector t (with displacement magnitude $|t|$) is expressed as:

$$R = 1 + \frac{et}{2} \tag{26}$$

2.3.2. CGA representation and calculation methods. The 5-dimensional Conformal Geometric Algebra is an extension of the 4-dimensional Projective Geometric Algebra, in which spheres and circles can be involved as basic algebraic quantities. The Geometric Algebra has a total of three products: the geometric product, the inner product, and the outer product, where the outer product mainly serves to construct basic geometries or geometries intersections, while the inner product is used to solve for scalars such as distances and angles.

Introduce the origin e_0 and the infinity point e_∞ in the 3D Euclidean geometry basis vector e_1, e_2, e_3. And represent the point x in the 3D Euclidean geometry with the basis vector e_1, e_2, e_3 by using the outer product “∧” and the inner product is $e_1^2 = e_2^2 = e_3^2 = 1 e_0^2 = e_\infty^2 = 0 e_0 \cdot e_\infty = -1$:

$$x = x_1e_1 + x_2e_2 + x_3e_3 \tag{27}$$

2.3.3. Conformal Geometric Algebra in 3D Animation:

1) CGA description of human network modeling. The modeling background of 3D animation in this paper is to read the OBJ file on the Net development platform to show the 3D animation mesh model. The establishment of the model grid is mainly to read the OBJ file in each line of point coordinates, three adjacent point coordinates constitute a triangular slice, the entire OBJ file point coordinates constitute a number of different triangular slices, all the triangular slices together to show the three-dimensional human body model.

In order to observe the 3D animation modeling method more clearly, we select some of these points in red, between the three adjacent points constitute the triangular slices, the point coordinates of the model are described by Euclidean geometry, we need to convert these point coordinates into a conformal geometric algebraic representation.

The description of all points through the Conformal Geometry Algebra points is converted into the following expression: $P = x + \frac{1}{2}x^2 e_\infty + e_0$ The coordinates of the 3D animation model points read through the OBJ file are $x = x_1 e_x + x_2 e_y + x_3 e_z, e_x, e_y, e_z$ are the base coordinates of the Euclidean geometry, and $x^2 = x_1^2 + x_2^2 + x_3^2$ in the Conformal Geometry Algebra.

Substituting into the expression for the point coordinates of the Conformal Geometry Algebra yields:

$$P = x_1 e_x + x_2 e_y + x_3 e_z + 1/2(x_1^2 + x_2^2 + x_3^2)^2 e_\infty + e_0 \tag{28}$$

The coordinates of all points in the OBJ file are converted into algebraic expressions of conformal geometry according to the above calculation method.

2) Motion analysis of 3D human body models. From the top to the bottom are leg joint point P_0, knee joint point P_1 and ankle joint point P_2, the conformal geometric expressions for joint points P_0, P_1 and P_2 are respectively:

Leg joint point coordinates:

$$P_0 = x_0 + \frac{1}{2}x_0{}^2 e_\infty + e_0 \tag{29}$$

Knee point coordinates:

$$P_1 = x_1 + \frac{1}{2}x_1^2 e_\infty + e_0 \tag{30}$$

Ankle joint point coordinates:

$$P_2 = x_2 + \frac{1}{2}x_2{}^2 e_\infty + e_0 \tag{31}$$

The skeleton between the leg joint to the knee joint point is a straight line L_1 and the skeleton between the knee joint point to the ankle joint point is a straight line L_2.

The distance between the leg joint to the knee joint and the knee joint to the ankle joint:

$$\left|L_1 L_2\right| = \sqrt{-2(L_1 \cdot L_2)} \tag{32}$$

When the leg completes the leg lifting motion, it is a rotational process that the skeleton between the knee joint point and the ankle joint point is rotated with the Z-axis as the axis and the leg joint point as the vertex, and the rotated knee joint point is $P_1^{'}$, the ankle joint point $P_2^{'}$, the skeleton between the leg joint to the knee joint point is a straight line $L_t^{'}$, and the skeleton between the knee joint point to the ankle joint point is a straight line $L_2^{'}$.

The model motion calculation in this topic is divided into two cases: the first one is to give the initial position of the model skeleton and the motion angle of the skeleton, and solve the position of the points after the motion of the skin mesh points bound to the skeleton. In the second one, the initial position of the model skeleton and the position of the skeleton after motion are known, and the motion angle of the skin mesh points bound to the skeleton is solved.

Point P is any point of the skin mesh, after the skin mesh is bound to the skeleton, point P will move together according to the skeleton, to solve the position of the skin mesh firstly find the position of the joints, the angle of rotation in the first step θ, as well as the angle of rotation in the second step α, and the post rotation coordinate point of the skeleton by $\theta = \arccos\frac{P \cdot S}{|P| \cdot |S|}$. Skeleton distance $|L_1| = -2(P_0 \cdot P_1), |L_2| = -2(P_1 \cdot P_2)$.

To calculate the skin mesh deformation outside the skeleton, we first need to know the rotation angle $\alpha_i = \alpha_i^\theta - \alpha_i^\beta$ of each joint point, where α_i^θ denotes the current rotation angle of the joint point t, and α_i^β denotes the rotation angle at the bound position, and in general, the rotation angle is generally obtained by rotating around the local coordinate axes, and then the final rotation angle is calculated for the skin fixed point P:

Let L be the distance from the skin mesh point to the skeleton, the weight of the mesh in the skeleton skinning animation is calculated as:

$$w_i(p) = \prod_{\substack{j=0 \\ (j \neq i)}}^{n} L^m / \sum_{k=1}^{n} \prod_{\substack{j=0 \\ (j \neq k)}}^{n} L^m \tag{33}$$

In the above equation, n is the maximum number of affected joints per skin mesh vertex, and m is the descent rate.

3. Results and discussion

3.1. Stage keyframe extraction experiment

3.1.1. Non-uniform chunking of images. Traditional video keyframe extraction, you can consider the video character object extraction after keyframe extraction according to the content of the video character. Animated video is very different from traditional video in production, resulting in animated video has its own obvious characteristics. For example, in animated video, the movement rate of the target object is faster than the general video, and in order to highlight the effect, the video generally pays more attention to the exaggerated performance of the action and expression. These exaggerated techniques make the target extraction algorithm less effective and less feasible.

Most of the traditional video is recorded and edited, while the animation video is often the first design of the animated character's movements, in the research process found that a considerable number of animated video footage of the background is relatively fixed a lot of footage containing complex actions whose background is relatively maintain a high degree of similarity, or even a fixed static image background. Experiments on the current mainstream Disney animation, Japanese animation, Chinese animation three types of animation video lens type statistics. The animation video lens background type statistics are shown in Table 1. As can be seen from the statistics table, more than half of the selected animation videos have a static image background, which is an important feature of animation videos. For example, the proportion of static background in Disney animation is 60.11%. Object and background separation method, i.e., video frames are subjected to non-uniform image chunking, so that the image frame is divided into the target object region and the background region.

Table 1. Animation video background type statistics

	Disney animation	japanimation	Domestic animation	Total
Lens number	559	312	388	1259
Static background	336	182	221	739
Dynamic background	223	130	167	520
Static proportion	60.11%	58.33%	56.96%	58.7%

3.1.2. First stage keyframe extraction. Aiming at the characteristics of animated videos with a large number of static backgrounds, it is proposed to first perform image chunking on video frames, and then filter a large number of highly similar video frames within the same scene by calculating the feature distance of the background region. The first stage of keyframe extraction is mainly to extract alternative keyframes, and the computational complexity of the algorithm is the main consideration. The above mentioned image non-uniform chunking method divides the background into three different regions, the background region 2 and background region 4 are easily affected by the station label, video subtitles or other factors, the experiment selects the background region 3 as a representative for feature distance calculation. The selection of feature distance, the first stage of the candidate key frame extraction to select the pixel difference as the feature distance, simple and easy to realize. The experimental study found that the R, G and B components of pixel difference are highly similar, and the R component is used to calculate the pixel difference between frames in the experiment. The comparison of background and inter-frame mutual information volume features is shown in Fig. 6 where Fig. a shows the background R-component feature distance and Fig. b shows the video inter-frame mutual information volume features. As can be seen from the figure, most of the shots in the background feature distance are clearly demarcated, and in order to avoid losing the key information, the threshold setting should be relatively strict. By setting a strict threshold for the first stage of alternative key frame extraction can filter a large number of highly similar video frames and reduce the number of video frames.

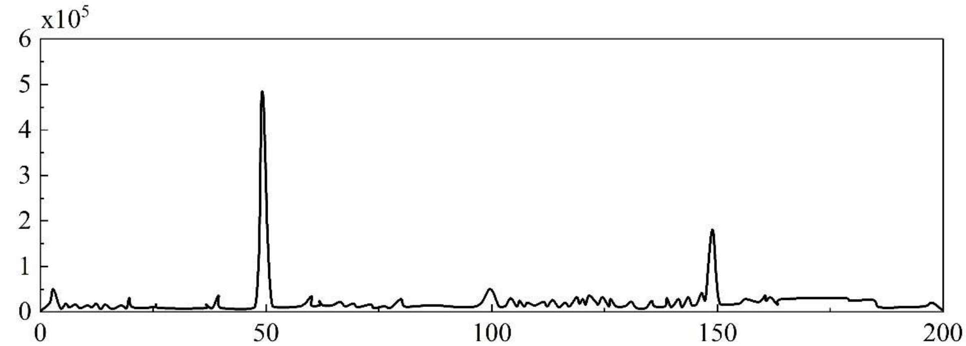

(a) Background R component characteristics distance

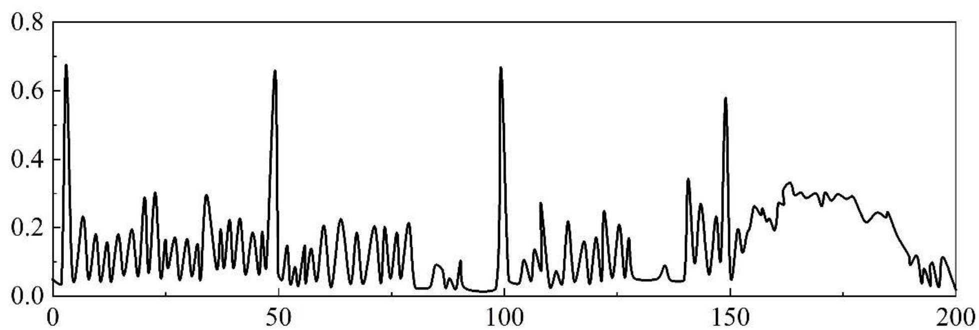

(b) The mutual trust rate feature of video frame

Fig. 6. The background is compared with the mutual trust rate

3.2. Experimental results of 3D animation keyframe interpolation algorithm

The algorithm of this paper is implemented. The system environment is CPU with 512M memory and the development environment is VC++6.0.The interface of the animation module of our system is shown in Fig. Examples of some of the interpolation results are given in Fig. 7 and Fig. 8 (a denotes the input start and end keyframes, b denotes the first frame of interpolation, c denotes the second frame of interpolation, and d denotes the third frame of interpolation).

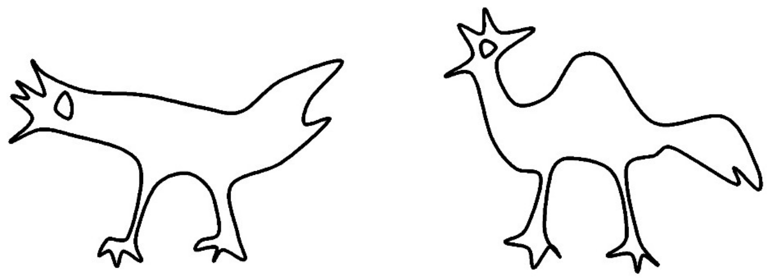

(a) Enter the starting and end key frames

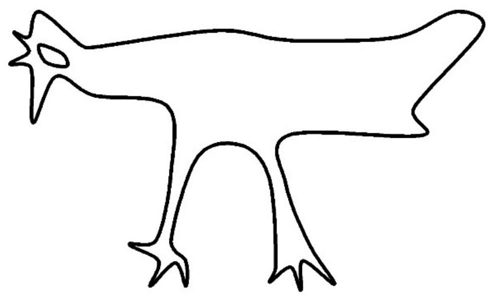

(b) Interpolation first frame

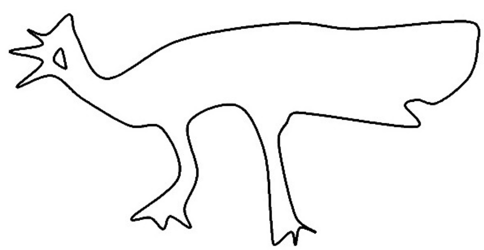

(c) Interpolation second frame

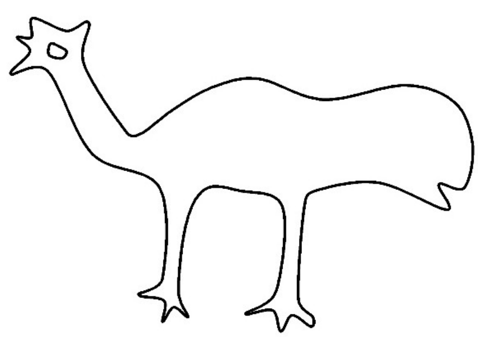

(d) Interpolation third frame

Fig. 7. Interpolation 3 frames after sequence

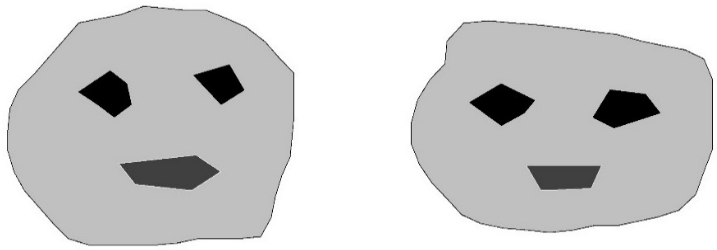

(a) Enter the starting and end key frames

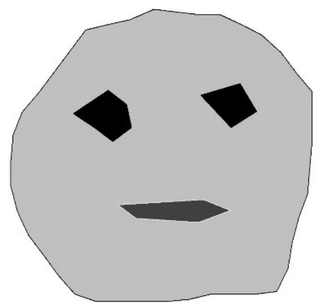

(b) Interpolation first frame

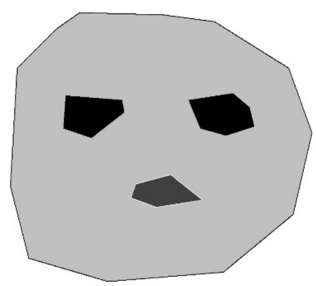

(c) Interpolation second frame

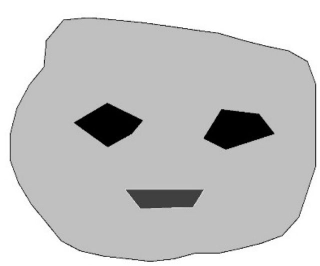

(d) Interpolation third frame

Fig. 8. Interpolation 3 frames after sequence

3.3. 3D animation modeling effect analysis

3.3.1. Comparison of 3D reconstruction results. In order to rigorously compare the 3D human reconstruction quality of various models and to prove the generalization degree of this paper's model, the experiments in this paper use the evaluation indexes of mean joint point coordinate error MPJPE and reconstruction loss error Reconst. Error for the comparison. The smaller the values of MPJPE and Reconst. Error are, the better the 3D reconstruction algorithm of human body is. The comparison of reconstruction errors of different models in Human3.6M (Protocol 2) test set is shown in Table 2. Comparison of the average joint error of different models in Human3.6M (Protocol 1) test set is shown in Table 3. Where the evaluation index data results of the comparative models are the results obtained by downloading their original models on the web with their published corresponding weight files and testing them under the same basic conditions of the experimental equipment. As can be seen from the table, the reconstruction algorithm in this paper has achieved good results in the two evaluation indexes, compared to SPIN, which has the largest reconstruction error, the method in this paper can even reduce the error of 36.8mm, so comprehensively this paper's method in the three-dimensional human body modeling effect is better than the above algorithms.

Table 2. Different models are compared to the test set reconstruction error

Method	Reconst. Error (mm)
SMPLify	82.2
NBF	60.2
GraphCMR	76.2
SPIN	94
METRO	87.2
Ours	57.2

Table 3. The different models were compared in the test set

Method	MPJPE (mm)
NeRF	88.57
SMPL	87.59
VIBE	80.35
Deep Kinematic Pose	106.95
HMR	87.54
Ours	85.23

3.3.2. Human Body 3D Mapping Model Generation Based on Surface Subdivision and Texture Mapping:

1) Implementation of the algorithm. In the 3D human reconstruction method based on the attention mechanism and graph convolutional network, the accuracy of the generated human body pose and shape has been improved compared with the classical algorithm, but compared with the input image, the personalized features of the character such as human appearance, hair style, clothing and texture are missing. In this paper, we consider the surface refinement of the original model to add the ability to express the details of the human body model surface to increase the normal mapping and displacement mapping, the growth of personalized features of the model, to further improve the algorithm, different algorithms for model vertex and face piece number of information as shown in Table 4.

Table 4. Different algorithm model vertices and processing information

Model name	Model vertex number	Model number
model	6899	13778
Add texture mapping model	27654	56217

2) Mapping reconstruction results for different human bodies. We have done a quantitative evaluation

of the mapping results generated in this paper to analyze the degree of advantages and disadvantages of the methods from an objective point of view. The comparative information of the time required to generate the texture maps is shown in Table 5. The experimental average time for generating texture mapping is 16.8s, and it takes a total of 16.8s to generate a 3D model containing detailed textures of the human body.

Table 5. The time compared to the generated map

Sample	Generate texture mapping time (s)
Enter the body 1	16.3
Enter the body 2	17.6
Enter the body 3	15.2
Mean time	16.8

The 2D joint errors of different algorithms are shown in Fig. 9. It can be seen that our algorithm compared to the classical HMR and SMPLify algorithms, the 2D joint error is reduced by 1.68mm and 0.5mm respectively, and the error of the 2D joint points can be further reduced, and it can be seen that the method in this paper has better reconstruction results than the other algorithms in the table compared to the previous algorithms.

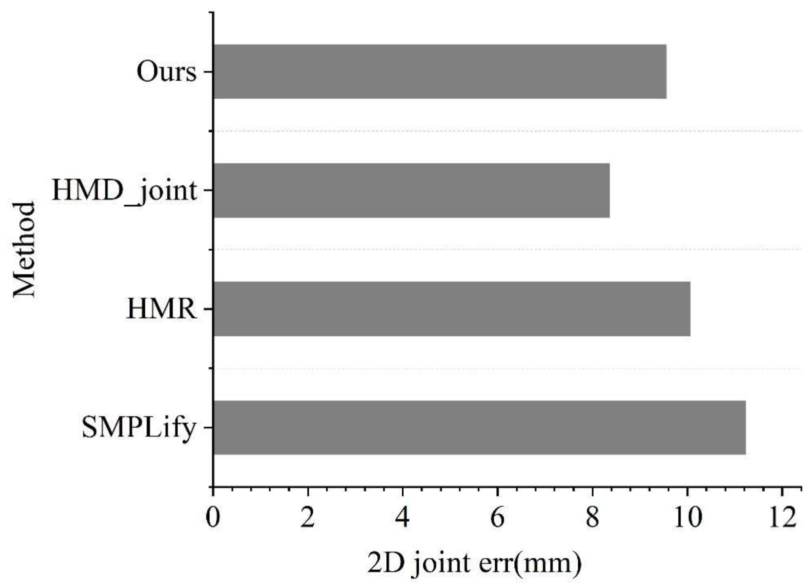

Fig. 9. Two-dimensional joint error of different algorithms

The time required for reconstruction by different algorithms is shown in Figure 10. As can be seen from the figure, the time required for reconstruction by our algorithm has been reduced considerably compared to the BodyNet algorithm, which can reconstruct the details of the human body, and compared to the HMR and VIBE algorithms, which can only predict the shape and pose of the human body of the image, our algorithm successfully predicts the details of the human body, even though it takes a little more time.

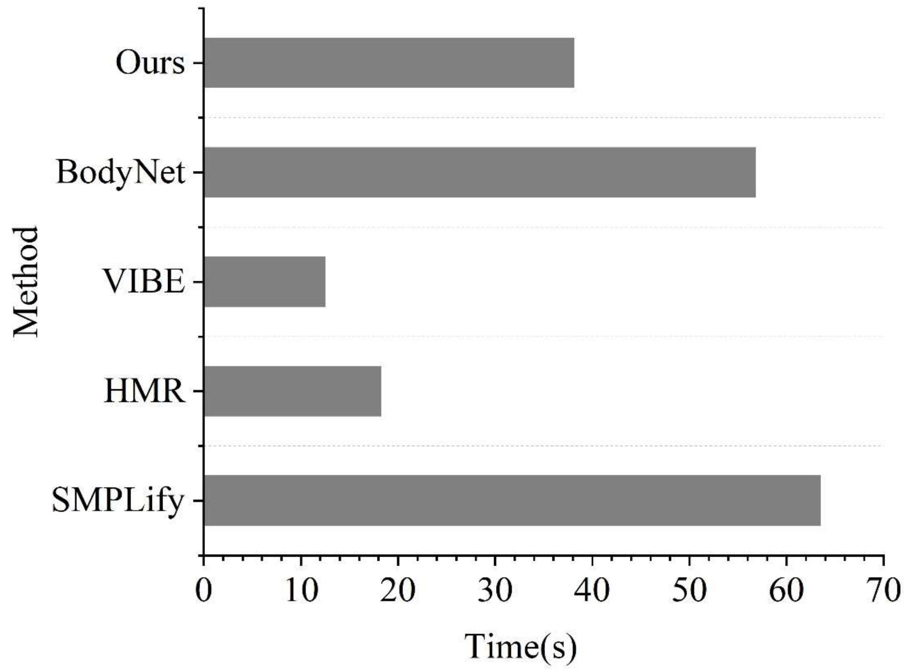

Fig. 10. The time required for the reconstruction of different algorithms

3.4. 3D Animation Visual Effects Analysis

3.4.1. Subjective evaluation of visual effects of 3D animated videos. Randomly selected 20 people in the age group between 25-45 years old were evaluated, including 10 expert users and 10 ordinary users, who subjectively evaluated the animation of 3D modeling using the method of this paper under the same viewing conditions, and the final evaluation results are shown in Fig. 11 (A denotes the video clarity discrimination, B denotes the video realism discrimination, C denotes the video spatial stereoscopic sense discrimination, D represents the video motion smoothness discrimination, and E represents the video lens comfort discrimination). As can be seen from the figure, the vast majority of people think that the animation video is clear, real, spatial stereoscopic sense, smooth movement of objects, and comfortable use of the lens. For example, 19 people think that the video has a strong sense of spatial three-dimensionality.

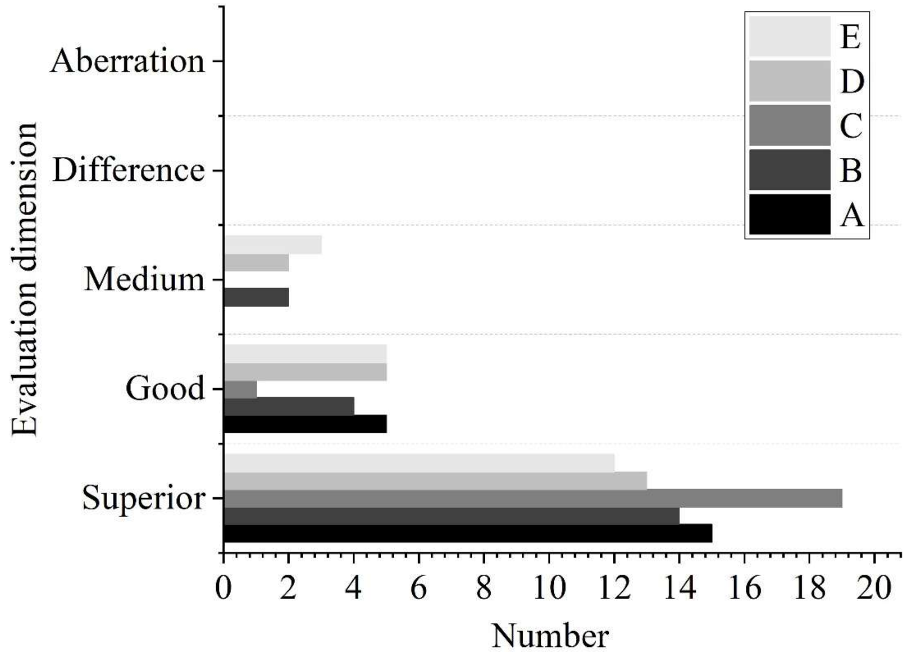

Fig. 11. Final evaluation

3.4.2. Multi-dimensional detection of 3D animated interface quality. On this basis, we choose 3D Monitor software to carry out multi-dimensional detection on the animation of 3D design using the method of this paper, in which the video size is 1920×1080, the video length is 120 seconds, and when the value is between 0-7, it shows green. When the value is between 8-13, orange color is shown. When the value is between 14-15, red color is shown. The specific values of the 3D video detection and analysis results in 3D Monitor software are shown in Table 6. It can be seen that all the frames satisfy the characteristics of visual comfort and stereoscopic sensation of the human eye, except for a very few frames for which false warnings are given, for example, in the luminance information dimension, the average value is 7.84.

Table 6. 3d video detection analysis results in 3d monitor software

Frame number	6	7	8	9	10	11	12	13	14	15	16	17	18	19	20	21	22	23	24
Brightness information	7	7	7	7	7	8	8	8	8	8	8	8	8	8	8	9	8	8	9
Color information	5	5	5	5	5	5	5	5	5	5	5	5	5	5	5	5	5	5	5
Vertical deviation	0	5	5	5	5	5	5	5	5	5	5	3	5	5	5	5	5	7	5
Different steps	0	0	0	0	0	0	0	0	0	0	0	0	0	0	0	0	0	0	0
Parallax deviation	0	0	0	0	2	0	0	0	2	0	0	1	0	2	4	4	0	0	0
Stereophony	0	0	0	0	0	0	0	0	0	0	0	0	0	0	0	0	0	0	0
Weak depth	0	0	0	0	0	0	0	0	0	0	0	0	0	0	0	0	0	0	0
Rich depth	2	8	8	8	8	8	8	8	8	8	8	8	8	8	7	8	8	8	8
Overconverging	0	4	4	4	4	4	4	4	4	4	4	4	4	5	2	3	3	3	3
Overdivide	8	8	8	8	8	8	8	8	8	8	7	7	7	7	7	7	7	7	7
Focal gap	0	9	6	6	6	6	6	7	7	6	6	6	7	7	6	5	8	8	8

3.4.3. New Visual Attention Modeling Quality Evaluation Measure Data Tests. The Video Quality Expert Group (VQEG) is dedicated to the testing and performance evaluation of different video quality algorithms.VQEG has a dedicated video quality testing device, to which raw uncoded videos (without dedicated video sequences) and processed videos can be input as the video under test, and the reference values of video quality are obtained by real-time computation.

First, we compress the videos selected to participate in the experiments, classified as: HIGH QUALITY and LOW QUALITY, and use the new visual attention model proposed earlier in two pixel-domain based quality evaluation measures, PSNR and SSIM, in the VQEG database. The scatterplot and nonlinear curve fitting of the proposed method in this paper on the VQEG database are shown in Fig. 12. From the figure, it can be seen that the method of this paper has a larger correlation coefficient with subjective perception relative to the previous method, and the weighted algorithm has a larger improvement over the full-reference type of PSNR and SSIM, and it is more consistent with the perceptual characteristics of the human eye which is more sensitive to the contour information and motion information of the objects in the video, so the 3D animation modeling technique based on geometric algebra has a better visual propagation effect.

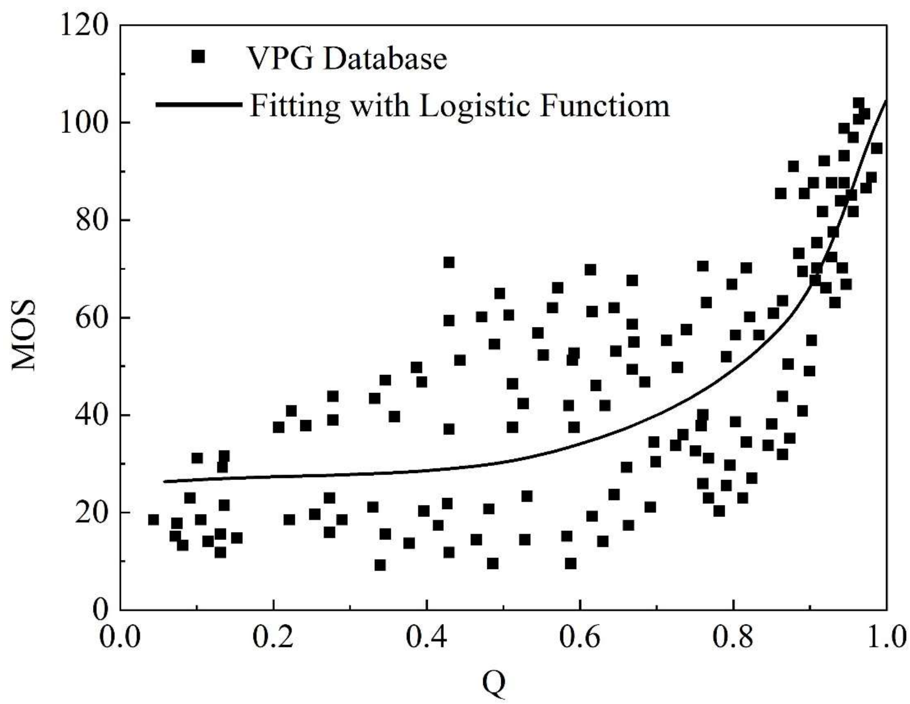

(a) PSNR

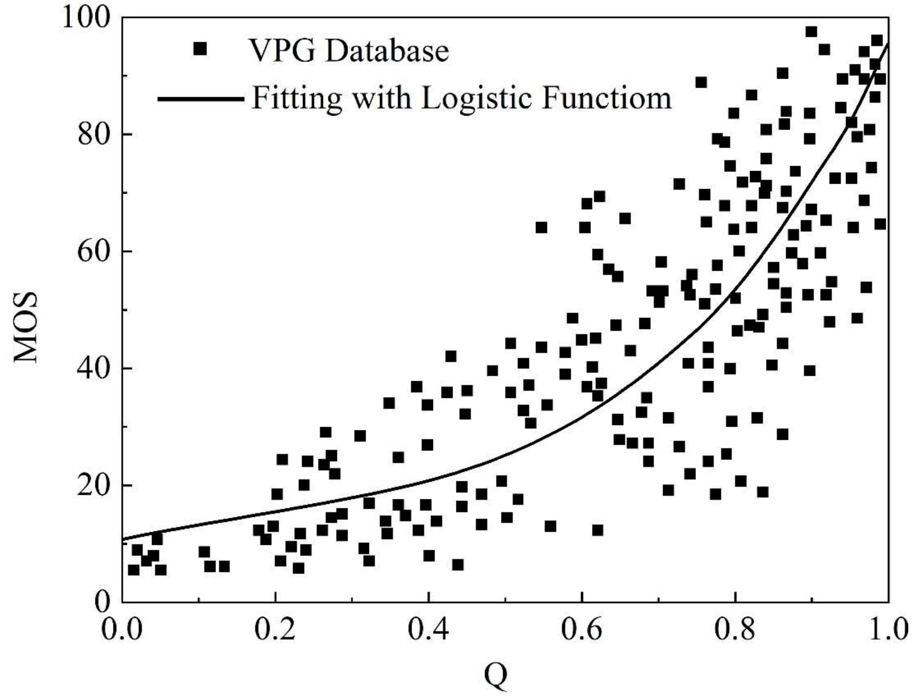

(b) Proposed

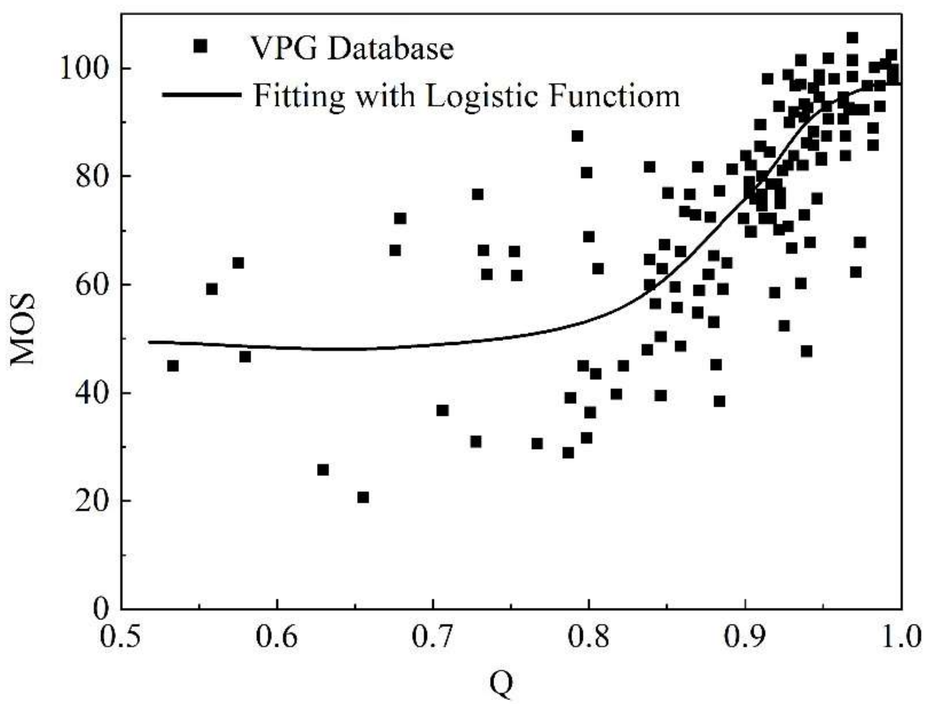

(c) SSIM

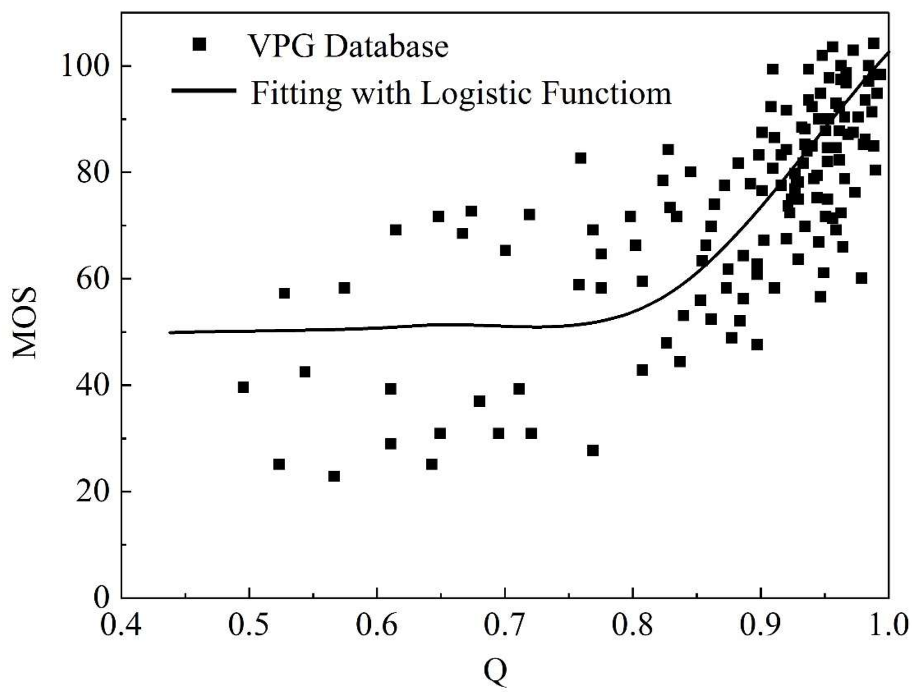

(d) Proposed

Fig. 12. The scatter point diagram and the nonlinear curve fit

4. Conclusion

This paper applies the geometric algebra method to 3D animation modeling, and verifies through relevant experiments that the method in this paper is more accurate in 3D animation modeling and can obtain more accurate detailed features and good visual effects. Through experimental tests, the article draws the following conclusions:

The key frame algorithm is used in specific animation production, and it is found that the algorithm synthesized screen results are natural and smooth, with certain practical value.

After the modeling experiment comparison, it is found that compared with SPIN, which has the largest reconstruction error, the method in this paper even reduces the error by 36.8mm, and the experiment shows that the algorithm proposed in this paper is able to improve the accuracy of the model and also shows many details.

In summary, the 3D animation modeling technology proposed in this paper is designed in a more stable form with high video quality, which can provide a reference for the subsequent processing of animated images.

References

[1] Verykokou, S., & Ioannidis, C. (2023). An overview on image-based and scanner-based 3D modeling technologies. Sensors, 23(2), 596.

[2] Luan, X., Xie, Y., Ying, L., & Wu, L. (2008). Research and development of 3D modeling. IJCSNS International Journal of Computer Science and Network Security, 8(1), 49-53.

[3] Birbara, N. S., Otton, J. M., & Pather, N. (2019). 3D modelling and printing technology to produce patient-specific 3D models. Heart, Lung and Circulation, 28(2), 302-313.

[4] Huang, T. C., & Lin, C. Y. (2017). From 3D modeling to 3D printing: Development of a differentiated spatial ability teaching model. Telematics and Informatics, 34(2), 604-613.

[5] Livesu, M., Ellero, S., Martínez, J., Lefebvre, S., & Attene, M. (2017, May). From 3D models to 3D prints: an overview of the processing pipeline. In Computer Graphics Forum (Vol. 36, No. 2, pp. 537-564).

[6] Ntousia, M., & Fudos, I. (2019, June). 3D printing technologies & applications: an overview. In Proceedings of the CAD 2020 Conference, Singapore (Vol. 243, p. 248).

[7] Shahrubudin, N., Lee, T. C., & Ramlan, R. J. P. M. (2019). An overview on 3D printing technology: Technological, materials, and applications. Procedia manufacturing, 35, 1286-1296.

[8] Jing, Y., & Song, Y. (2020). Application of 3D reality technology combined with CAD in animation modeling design. Computer-Aided Design and Applications, 18(S3), 164-175.

[9] Josephson, S., Kelly, J., & Smith, K. (2020). Handbook of visual communication. Handbook of Visual Communication.

[10] Machin, D. (Ed.). (2014). Visual communication (Vol. 4). Walter de Gruyter GmbH & Co KG.

[11] Russmann, U., & Svensson, J. (2017). Introduction to visual communication in the age of social media: Conceptual, theoretical and methodological challenges. Media and Communication, 5(4), 1-5.

[12] Wang, R. (2021). Computer-aided interaction of visual communication technology and art in new media scenes. Computer-Aided Design and Applications, 19(S3), 75-84.

[13] Abd Rashid, M. H., & Md Johar, E. (2022). The Perceived Effectiveness of Visual Communication Elements in Cinema Video Advertisements: Demographic Factors Analysis. Journal of Social Science and Humanities, 5(4), 10-23.

[14] Chodak, G., Chawla, Y., Dzidowski, A., & Ludwikowska, K. (2019, June). The effectiveness of marketing communication in social media. In ECSM 2019 6th European conference on social media (p. 73). Academic Conferences and Publishing Limited Sonning Common, UK.

[15] Zhao, Q. (2018). The Application of Augmented Reality Visual Communication in Network Teaching. International Journal of Emerging Technologies in Learning, 13(7).

[16] Liu, W. (2021). Research on the application of multimedia elements in visual communication art under the internet background. Mobile Information Systems.

[17] Kiu, Z. (2020). The dynamic effect of visual communication in web design and its technical realization. Computer-Aided Design and Applications, 17(S2), 78-88.

[18] Yu, G., Akhter, S., Kumar, T., Ortiz, G. G. R., & Saddhono, K. (2022). Innovative application of new media in visual communication design and resistance to innovation. Frontiers in Psychology, 13, 940899.

[19] Na Jia. (2024). Indoor space thermal cycle design and animation 3D modeling based on digital light processing technology. Thermal Science and Engineering Progress102808-102808.

[20] Xiong Anya & Wang Qin. (2023). SOR Model and Application of Virtual Reality Technology in 3D Animation Design. Applied Mathematics and Nonlinear Sciences(2),1725-1734.

[21] Margarita Papaefthymiou,Dietmar Hildenbrand & George Papagiannakis. (2016). An inclusive Conformal Geometric Algebra GPU animation interpolation and deformation algorithm. The Visual Computer(6-8),751-759.

[22] Jiang Xiaomin,Huang Yangfei & Zhang Feng. (2022). Study on Spatial Geometric Similarity Based on Conformal Geometric Algebra. International Journal of Environmental Research and Public Health(17),10807-10807.